Electronics and Electrical Engineering

AIMS Electronics and Electrical Engineering, 8(4): 466–487.
DOI: 10.3934/electreng.2024022
Received: 24 August 2024
Revised: 18 October 2024
Accepted: 29 October 2024
Published: 20 November 2024

https://www.aimspress.com/journal/ElectrEng

Research article

Compact modified rectangular split ring resonator for tri-band satellite applications

Abderraouf Fadhel[1,2,*], Souad Berhab[3,4], Rahma Aloulou[1,2], Hassene Mnif[1,2,*] and Abdennour Belhedri[5]

[1] Laboratory of Electronics and Information Technologies, ENIS, University of Sfax, Tunisia
[2] National School of Electronics and Telecommunications (ENET'Com), University of Sfax, Tunisia
[3] Higher National School of Telecommunications and Information and Communication Technologies-ENSTTIC, Oran, Algeria
[4] LARATIC laboratory, ENSTTIC, Oran, Algeria
[5] Dept. of Electronic and Telecommunications, University of Kasdi Merbah Ouargla, Algeria

* **Correspondence:** Email: fadhel.abderraouf97@gmail.com (A.F), hassene.mnif@enetcom.usf.tn (H.M); Tel: +2136622177317 (A.F), +21674862500 (H.M).

Abstract: This paper contributes to the design of a modified rectangular-shaped metamaterial with a tri-band coverage for reflection and transmission coefficients. Two symmetrical rectangular split ring resonators (SRR) were carefully engineered and then connected by their edges along the axis (Ox) with a substantial C-shaped structure, experiencing the peak surface current value near the magnetic resonances, causing the proposed unit cell to resonate at 5.73 GHz, 8.67 GHz, and 13.78 GHz, where it exhibited negative effective permittivity (ENG), permittivity and permeability (DNG), and permeability (MNG), respectively. A total of 6 × 6 mm^2 modified SRR was printed on Rogers RO3006 to achieve a better effective medium ratio (EMR) in the C band (4.55-6.27 GHz), X band (7.81-9.45 GHz), and Ku band (13.15-14.37 GHz), respectively. A comprehensive parametric analysis was performed to illustrate the effect of crucial parameter h on the scattering parameters (S_{11}, S_{21}) of the metamaterial resonant structure (MRSRR) in the specified frequency ranges. Structure underwent additional testing with 1 × 2, 2 × 1, 2 × 2, and 4 × 4 arrays, yielding results that demonstrated sufficient concordance for consideration in the C band [4-8 GHz], X band [8-12 GHz], and Ku band [12-18 GHz] satellite applications. Computer Simulation Technology (CST) Microwave Studio was utilized to reach the scattering parameters and their effective medium characteristics, specifically permittivity and permeability, via the Nicolson–Ross–Weir (NRW) approach, executed through MATLAB code. The surface current was examined, and the corresponding circuit model was

confirmed utilizing the Advanced Design System (ADS) software, with results compared against the CST simulation outcomes.

Keywords: effective parameters; satellite communication; metamaterial; Nicolson-Rose-Weir (NRW)

1. Introduction

Metamaterials (MTMs) or artificial media have several special properties concerning electromagnetic waves. They demonstrate remarkable functional performance in various fields, including the absorption, emission, sensing, transmission, and guiding of light, sound, energy, heat, friction, strength, and electric energy [1]. Their unique properties have captivated scientists looking to address issues in antennas and microwave circuits. MTMs are composite structures called cells that are artificially arranged and embedded in a base medium, generally of the dielectric substrate. Cells' special geometries let metamaterials show contradictory electromagnetic characteristics, which makes them quite attractive for use in technology. It is feasible to control the permittivity and permeability by changing parameters like cell size, shape, and arrangement to attain planned properties [2]. These characteristics mainly consist of homogeneity since the cells are much smaller than the operational wavelength, guaranteeing constant performance over several frequencies.

Near the end of the 19th century, researchers first pursued the idea of synthetic materials. In 1898, Bose JC conducted the inaugural microwave experiment, employing twisted synthetic fibers to manipulate the polarization of electromagnetic waves generated by a liquid, such as a sugar solution. Victor Veselago first proposed metamaterials, also known as Left-handed Materials (LHM), in 1967. These materials comprise an indirect trio of vectors: Phase propagation, electric field, and magnetic field [3]. Pendry et al. introduced the innovative idea of creating materials with negative permittivity using metallic wires in 1996. Pendry J proposed a method to reduce the electrical plasma frequency. They used a regular pattern of thin metal wires and air spaces between them. This technique out the metal and lowers the electron density by creating an effective medium, which the Drude model says.

Furthermore, a current traversing the metal rods generates a magnetic field that influences the charges by increasing their effective mass. The simultaneous impact of medium dilution and the rise in effective mass facilitates a decrease in the electrical plasma frequency. Therefore, developing a material with negative permittivity is suitable for use in the microwave domain [4]. The prospect of developing non-magnetic materials that exhibit a magnetic reaction is truly inspiring. In 1999, Pendry and his colleagues realized the Swiss roll structure. The same team suggested adding the Split Ring Resonator (SRR) to improve the Swiss-Roll structure's absorption problems caused by the filling factor [5].

Two interlocked metal loops formed like the letter "C" with SRR-based designs have become essential in obtaining negative permeability in non-magnetic materials. A pillar in the evolution of several metamaterials, including antennas, absorbers, sensors, filters, and energy harvesting devices [6–11], use the SRR's capacity to control electrostatic energy has made all the difference.

Very rare or nonexistent in nature, Single Negative (SNG) and Double Negative (DNG) qualities can be possessed by metamaterials [12]. Conversely, natural materials generally have double positive permittivity and permeability (Double Positive Media, DPS). Research such as that performed by Al-Gburi et al. [13] and Sharma et al. [14] show the useful applications of DNG metamaterials in wideband and shielding technologies. Sabaruddin et al. [15] engineered a highly sensitive five-band absorber employing metasurfaces in the terahertz spectrum. The absorber

functions effectively in terahertz imaging, sensing, and detecting systems. Chou Chau examined methods to enhance the efficiency of second harmonic generation (SHG) by incorporating split-ring resonators and bowtie nanoantennas into metasurfaces. This significantly enhanced the nonlinear optical responses. These accomplishments show how metamaterials are necessary for new developments in photonic technology, electromagnetic protection, and telecommunications [16].

Diverse alphabetic metamaterial configurations for various applications have been reported in the literature. In [1], Alam and Latif developed a Double-Split Rectangular Dual-Ring, with a negative refractive index (DNG) for 5G millimeter-wave applications. This metamaterial was printed on Rogers RT/Duroid 5880 and has an effective medium ratio (EMR) of 3.76 at dimensions of 3.05 × 2.85 mm^2. Alam JB et al., a double negative modified H-shape was presented with an EMR of 15.33 at 12 × 12 mm^2 for satellite communication in reference [17]. Md Ikbal Hossain et al. [18] presented a Novel Wide-Band Double-Negative Metamaterial for C and S-band applications. The proposed cell exhibits double negativity in the C and S-Band and comprises two G-shaped split-square resonators connected and printed on FR-4 glass epoxy. Mohammad Shahidul Islam et al. [19] proposed a gap-coupled hexagonal split ring resonator-based metamaterial for S-Band and X-Band microwave applications with an EMR of 4.76. The proposed cell has dimensions of 10 × 10 mm^2 and is printed on inexpensive FR4 material. Almutairi AF et al. designed and investigated a metamaterial based on a CSRR (complementary split-ring resonator) [20]. The unit cell was printed on FR4 material and measured 5.5 × 5.5 mm^2. It featured a double negative region in C and X-Band, with an EMR of 8. A parallel double-E-shaped structure based on double negative (DNG) metamaterial for multiband applications is described [21]. The proposed unit cell has dimensions of 8 × 8 mm^2, and its substrate material is Rogers RT 5880. DNG metamaterial covers the S and C-band multiband frequencies with an EMR of 15.67.

As satellite communications change quickly, it is becoming increasingly important to have small, high-performance designs that can work with multiple bands. This paper proposes a novel compact resonator geometry suitable for satellite transmission systems. It possesses unique electromagnetic properties, operating in various frequency bands. To that end, the proposed unit cell operates as Epsilon Negative (ENG) in the C band, Double Negative (DNG) in the X band, and MU Negative (MNG) in the Ku band.

The unit cell uses a Rogers RO3006 substrate with a relative permittivity of 6.15 and a width of 1.28 mm. It has small dimensions of 6 × 6 mm ²and a high effective medium ratio (EMR) of 8.71. To enhance the design, we simulate array designs in sizes of 1 × 2, 2 × 1, 2 × 2, and 4 × 4 using CST Microwave Studio. The Nicolson-Ross–Weir (NRW) method calculates the electromagnetic properties and is used in MATLAB. Simulation with ADS software is employed to verify the analogous circuit. This multi-characteristic configuration may operate in DNG, ENG, and MNG modes, and it is reported to perform effectively across many satellite communication frequency bands.

The content of this study is organized into five sections. In Section 2, we outline the design technique for the modified rectangular SRR unit cell. In Section 3, we look forward to the simulation presentation and its corresponding results, including the validation of the MRSRR's electrical circuit model by comparing results acquired from CST and Agilent's ADS software. Additionally, in this section, we incorporate a study of the proposed unit cell in 1 × 2, 2 × 1, 2 × 2, and 4 × 4 arrays, followed by a comparison. In Section 4, we provide a comparison between the proposed unit cells and existing ones. Finally, in Section 5, we conclude the paper.

2. Proposed MTM unit cell

Figure 1(a) depicts the design of the modified rectangular split-ring resonator (SRR) simulated in CST Microwave Studio. C-shaped design, with a width D1, connects two symmetrically arranged two symmetrically positioned rectangular resonators, which are separated by D3, each with a width D2. Both sides of the unit cell have symmetric splits, each with a width of G2, positioned along the x-axis. Patch-MRSRR is affixed to a dielectric substrate measuring $Lp \times Wp$, as depicted in Figure 1(b). Resonators are fabricated from Rogers RO3006, which has a thickness of 1.28 mm, a relative permittivity of 6.15, and a loss tangent of 0.002. Copper strips with a thickness of 0.035 mm serve as the conducting medium. Split G2 introduces capacitance, while the metal strips produce inductance, establishing the structure's resonant frequency. The whole unit cell size is 6×6 mm^2. Table 1 presents the optimized dimensions of the metamaterial's unit cell (MTM).

Table 1. Geometrical parameters of the MRSRR unit cell.

Parameters	Values (mm)
Wp	6
Lp	6
G1	0.6
G2	0.1
D1	0.5
D2	0.4
D3	0.3

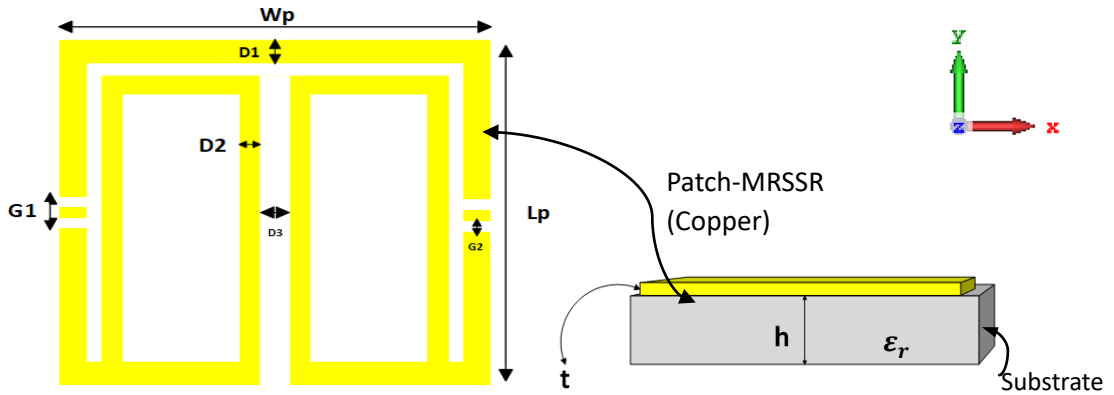

Figure 1. A MRSRR unit cell. (a) top view and (b) transverse view.

3. Simulation and results

3.1. Design and analysis

A simple model based on a simulation of the scattering parameters was investigated for finite structure analysis. The frequency domain solver (tetrahedral mesh), which has the time-harmonic dependence of the fields in Maxwell's equations [1], was explored. The normalized impedance was 50 Ω, and the simulation ranged from 1 to 20 GHz. Boundary conditions were used to imitate the periodic nature of the used cell [22]. In doing so, the MTM cell was positioned in front of the two

waveguide ports (1/2) along the opposite directions (±Oz), used to excite the unit cell. In directions of (±Ox) and (±Oy), PEC and PMC walls were used, respectively, as shown in Figure 2(a). It should be outlined that the cell had a symmetric shape, so permutation in PEC and PMC directions could be considered.

Incident TEM wave approached the patch in the (±Oz) direction from all directions. This resonance in the transmitted and reflected waves resulted from electromagnetic interaction inside the unit cell. These were excited by incident electromagnetic waves as they came in contact with the patch. The S-parameters of the MRSRR unit cell could be measured using coaxial cables to connect the unit cells to a Vector Network Analyzer, as shown in Figure 2(b).

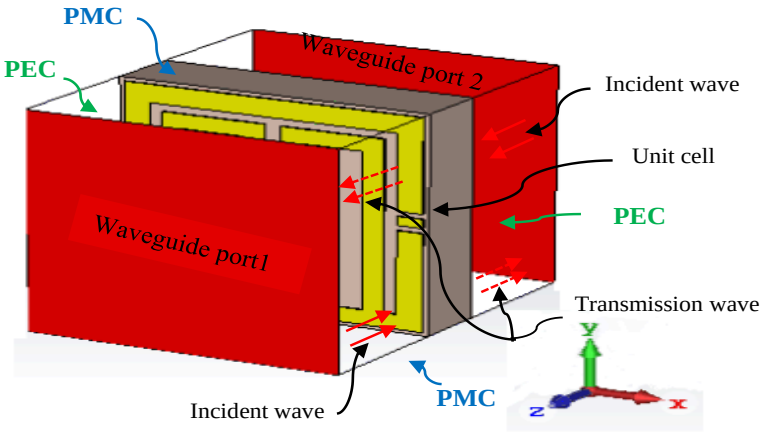

(a)

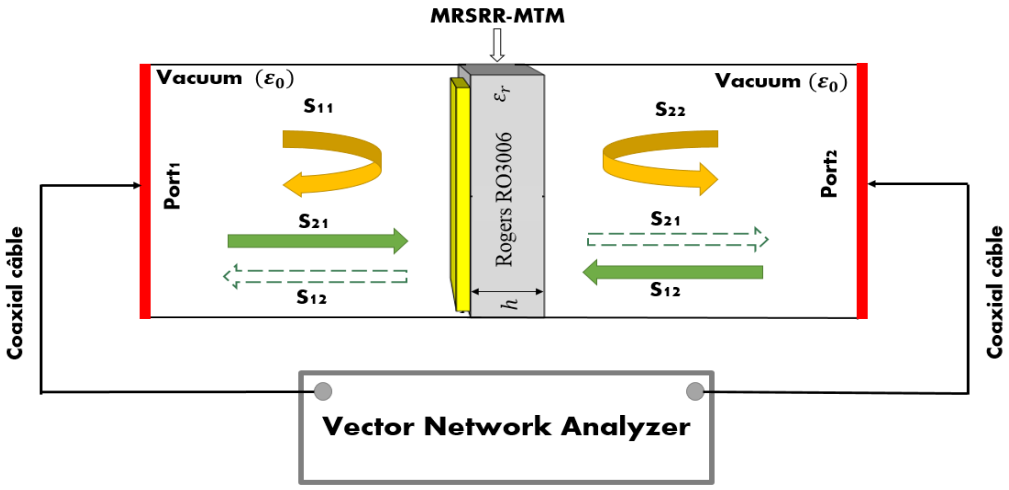

(b)

Figure 2. (a) the boundary condition for the proposed metamaterial unit cell. (b) a schematic diagram of the measurement method.

Based on the Finite Integration Technique (FIT), the CST was used to numerically simulate the modified RSRR unit cell. Figure 3 shows the scattering characteristics (S_{11} and S_{21}) graph of the suggested unit cell in the frequency range [1–20 GHz].

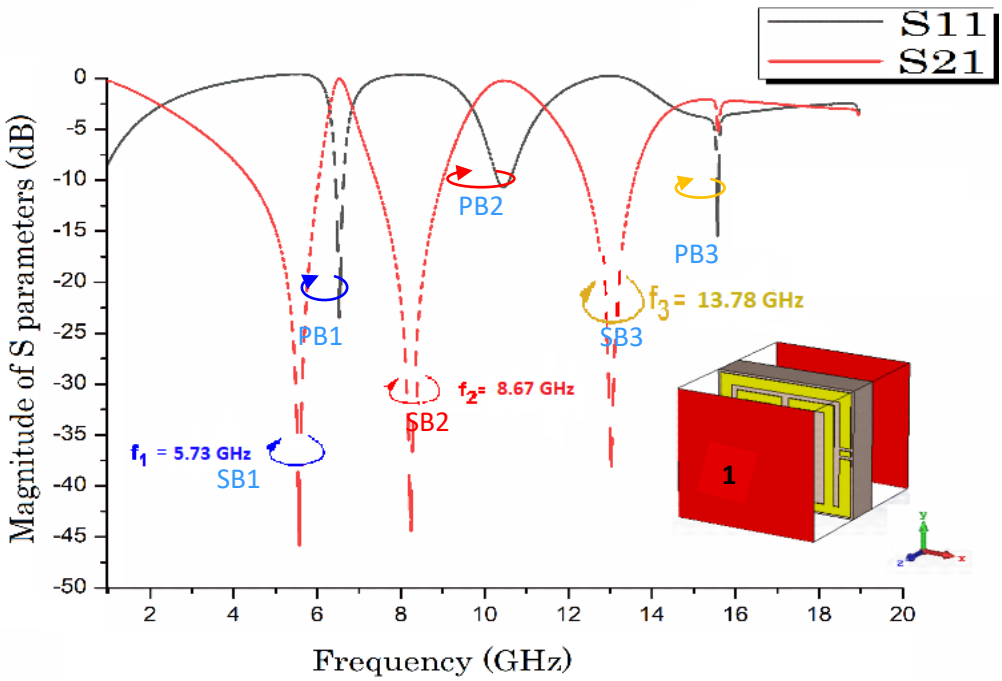

Figure 3. Scattering parameters of the MRSRR in the frequency range [1-20 GHz].

The transmission coefficient (S_{21}), illustrated graphically in Figure 3, picked the resonance frequencies of the MRSRR. The results indicated that triple resonances of the MRSRR were 5.73, 8.67, and 13.78 GHz, respectively. The transmission coefficient (S_{21}) was less than -10 dB, indicating three stopband characteristics (SB1, SB2, SB3). However, reflection coefficients (S_{11}) within the frequency bands (SB1, SB2, SB3) were practically 0 dB, meaning wave propagation was impossible [23].

Stopband responses (S_{21}) were around 5.73 GHz, 8.67 GHz, and 13.78 GHz, accompanied by excellent impedance matching, with readings of less than -35 dB and magnitudes of -46.01, -42.49, and -35.93 dB, respectively. MRSRR introduced bandwidths of transmission coefficient from 4.55 to 6.27 GHz, 7.81 to 9.45 GHz, and 13.15 to 14.37 GHz, with fractional bandwidths (FBW) of 30%, 18.91 %, and 8.85 %, respectively. Moreover, SB1 produced the wider stopband region. Additionally, the smallest was by SB3, as FBW indicated. Similarly, MRSRR indicated three passband characteristics (PB1, PB2, PB3) around 6.85 GHz, 11.02 GHz, and 15.65 GHz, respectively, accompanied by S_{11} magnitudes of -22.43 dB, -10.67 dB, and -15.32 dB, respectively.

The FBWs at 5.73 GHz, 8.67 GHz, and 13.78 GHz, respectively, were quantitative assessments of the bandwidths of the unit cell relative to their central frequencies. The consequence was the assessment of the MRSRR unit cell efficiency in terms of the rejection of signals at resonances. FBW was one of the most frequently used parameters of microwave design for representing the relative bandwidth of a signal or system. It was mathematically computed as:

$$FBW = \frac{\Delta f}{f_c} \quad (1)$$

Where:

Δf: Bandwidth of the MRSRR unit cell at -10 dB (-10 dB BW). It is commonly described as the difference between the upper and lower frequencies, based on the S_{21} magnitude being less than -10 dB.

Fc: Center frequency, defined as the mean of the higher and lower cutoff frequencies.

3.2. *Examining the effect of thickness h*

The specific design parameters studied substantially affected the effectiveness of the MRSRR's scattering properties (S_{11}, S_{21}). Rogers RO3006 was offered in many commercial thicknesses: h = 0.13 mm, h = 0.25 mm, h = 0.64 mm, and h = 1.28 mm, influencing the MRSRR's performance differently. Figures 4(a-b) demonstrate the effect of increasing thickness h on S_{11} and S_{21} responses, respectively.

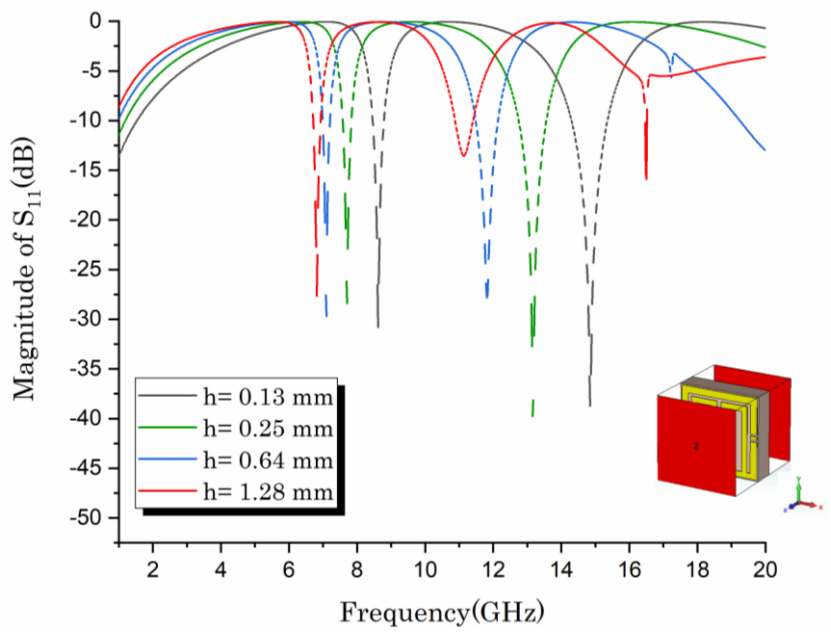

(a)

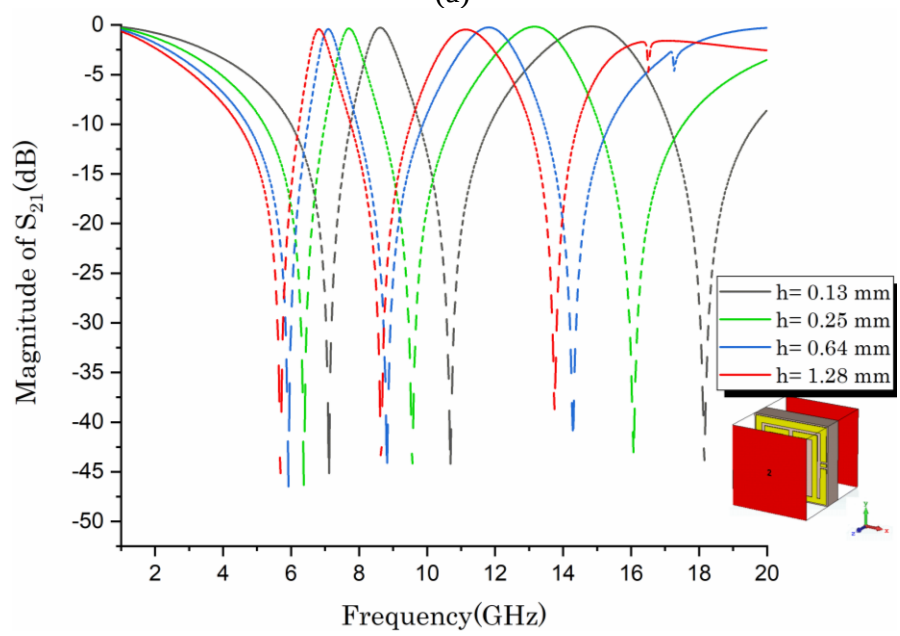

(b)

Figure 4. The magnitude of the MRSRR S-parameters (a) reflection coefficient S_{11} (dB) and (b) transmission coefficient S_{21} (dB).

Figure 4 illustrates that the resonance frequencies of the MRSRR unit cell were influenced by

the alteration of parameter *h*. Resonance frequencies increased significantly as substrate height decreased. A reduced *h* value diminished the total effective dielectric constant, thereby elevating the structure's resonance frequencies, aligning with theoretical predictions.

Smaller *h* decreased the overall effective dielectric constant, increasing the structure's resonance frequency, as expected from the theory. A total of 1.28 mm corresponded to an optimum between small thickness and good electromagnetic performance for frequencies of interest.

Nicolson-Ross-Wier (NRW) is a highly efficient and non-repetitive method, typically employed to retrieve the effective dielectric parameters (ε, μ) due to its suitability as a direct refractive index retrieval (DRI) method.

The Rose-Weir method is a widely used approach in materials characterization. It was created by Nicolson and Ross and showcased in their book "Measurement of the Intrinsic Properties of Materials by Time-Domain Techniques" in 1970. Metamaterials were analyzed using this efficient technique, as Smith et al. demonstrated in [24]. The NRW approach involves deriving the refractive index η, wave impedance Z, and effective parameters of composite medium from either measured or simulated parameters. The method choice is motivated by the ability to guarantee fast and accurate results. The following equations are used [25].

$$\Gamma = \frac{(Z_0 - 1)}{(Z_0 + 1)} \tag{2}$$

Z_0: Relative impedance for effective permittivity and permeability, determined as follows

$$z_0 = \sqrt{\frac{\mu_r}{\varepsilon_r}} \tag{3}$$

S parameters are calculated as follows

$$S_{11} = \frac{(1-\Gamma^2)Z}{1-\Gamma^2 Z^2} \tag{4}$$

$$S_{21} = \frac{(1-Z^2)\Gamma^2}{1-\Gamma^2 Z^2} \tag{5}$$

From S parameters, we create two vectors, V_1 and V_2:

$$V_1 = S_{21} + S_{11} \tag{6}$$

$$V_2 = S_{21} - S_{11} \tag{7}$$

Effective parameters are calculated using the following equations:

$$\varepsilon_r = \frac{c}{j\pi fd} \times \frac{(1-V_1)}{(1+V_1)} \tag{8}$$

$$\mu_r = \frac{c}{j\pi fd} \times \frac{(1-V_2)}{(1+V_2)} \tag{9}$$

d: dielectric slab thicknesses, f: frequency band [GHz]

The flowchart in Figure 5 represents the MRSRR analysis process based on Nicholson-Ross-Weir (NRW) to determine the electromagnetic parameters of a dielectric material from the S_{ij} coefficients.

The effective medium parameters (ε, μ) of MRSRR are ascertained by deriving the real and imaginary components of S_{11} and S_{21} via the NRW approach, as indicated by Equations (2)–(5). MATLAB code employing the NRW approach is used to obtain the real and imaginary values of the effective medium attributes.

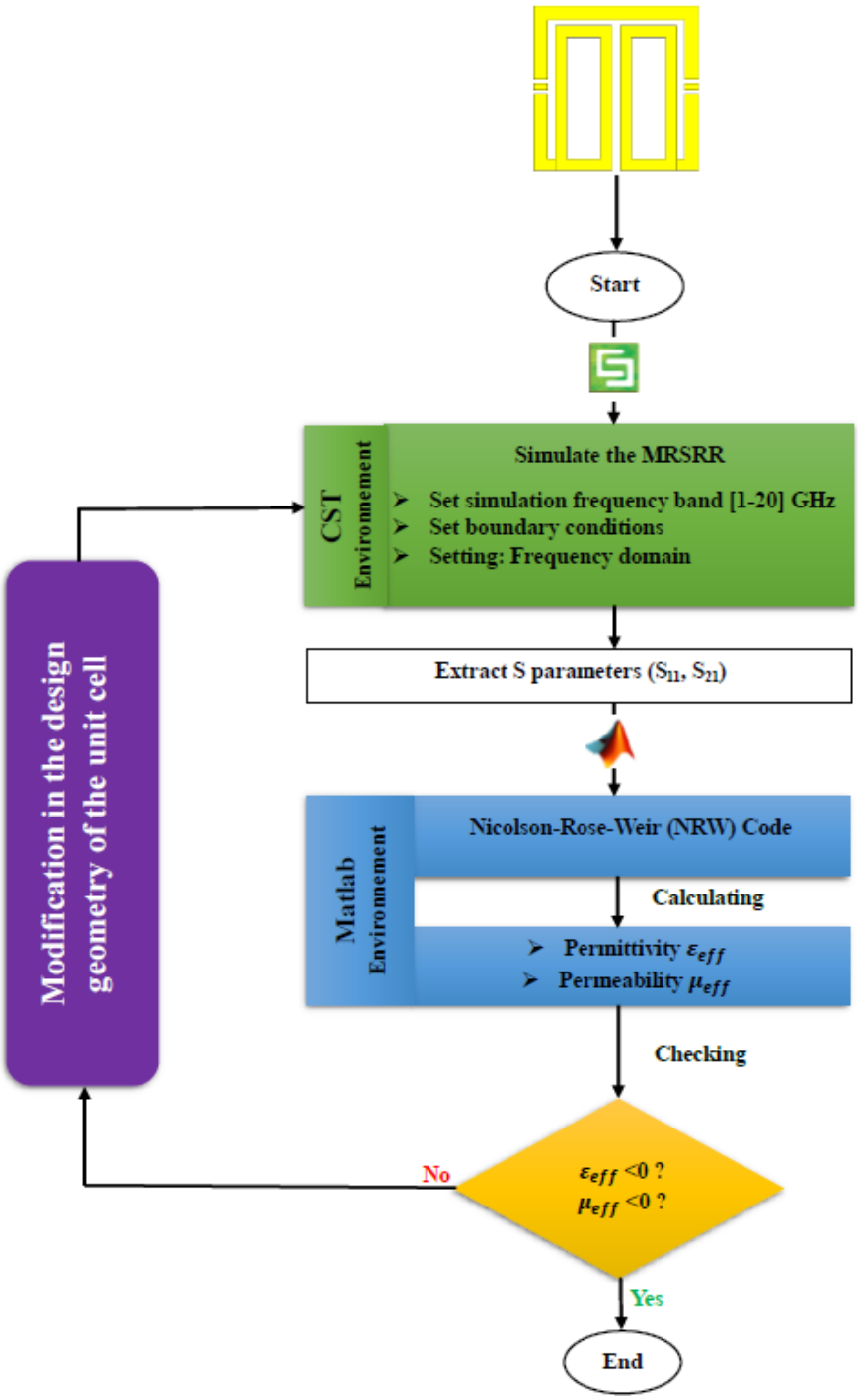

Figure 5. MRSRR analysis process based-NRW.

Figures 6(a) and (b) represent the results of effective permittivity and permeability, respectively, for the frequency range [1-20 GHz]. The plot shows that the real part of the effective permittivity had a negative value over the frequency range, starting from 4.25 to 6.24 GHz, 7.5 to 9.44 GHz, and 13 to 13.6 GHz. Negative permittivity values for frequency ranged from 7.1 to 9.9 GHz, and 11.9 to 13.8 GHz were also observed. It is clear from these figures that the imaginary part of either effective permittivity or permeability is positive within the cited frequency ranges, and hence, the criteria for metamaterial behavior are met. MRSRR stop bands (SB1, SB2, SB3) are responsible for the appearance of negative effective parameters.

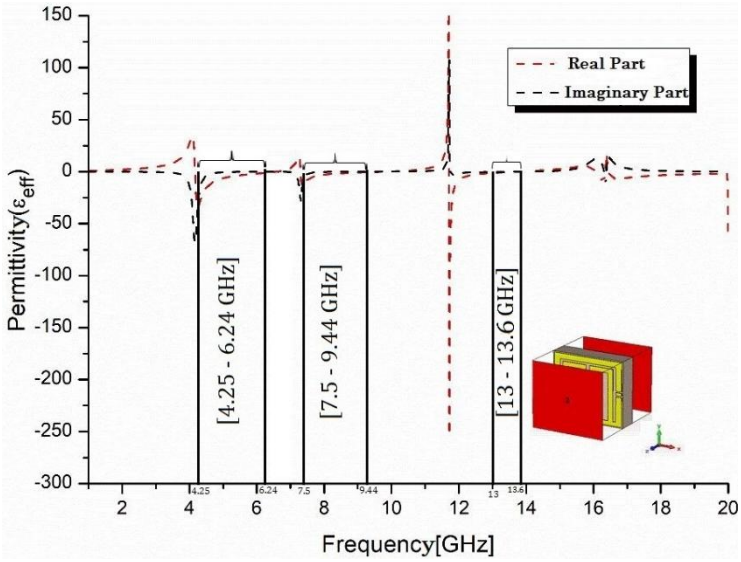

(a)

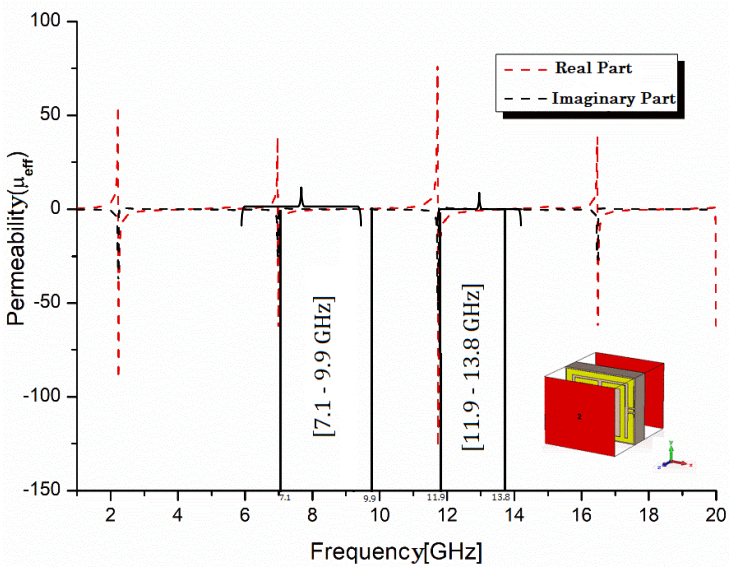

(b)

Figure 6. Effective parameters of the proposed unit cell (a) Permittivity and (b) Permeability.

Table 2 highlights MRSRR specifications in the frequency band [1-20 GHz].

Table 2. MRSRR specifications.

Resonance freq. [GHz] S_{21} **[dB] < -10 dB**	**ENG**	**MNG**	**DNG**	**Satellite covered bands**
f_{r1} = 5.73 GHz S_{21} = -46.01 dB	Yes	No	No	C
f_{r2} = 8.67 GHz S_{21} = -42.49 dB	Yes	Yes	Yes	X
f_{r3} = 13.78 GHz S_{21} = -35.93 dB	No	Yes	No	Ku

The surface current of the MRSRR-MTM unit cell for different transmission resonance frequencies is elaborated. Figure 7 shows the surface current distribution for three resonances at 5.73 GHz, 8.67 GHz, and 13.78 GHz, respectively.

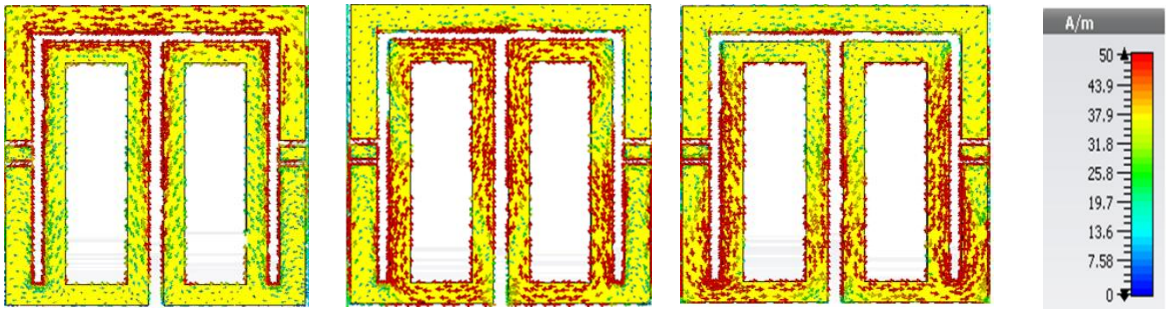

Figure 7. Surface current distribution of MRSRR at three resonance frequencies.

On the rings/metal segments, the surface current (electrical current) was the most prevalent. The conducting surface of the structure conducted a more significant amount of current than any other fundamental component. This current appeared symmetrical to the inner rectangular connected parts, indicated by the red color, and reached a maximum of 50 A/m, as shown in Figure 7. The splits of the rings regulated the current to rotate in opposite directions through symmetrical rings, resulting in stopband behavior at the resonance frequencies.

3.3. Electrical circuit model

MRSRR-MTMT is regarded as a passive LC circuit composed of passive components (inductance and capacitance). Resonance frequency can be calculated by:

$$f = \frac{1}{2\pi\sqrt{L_T C_T}} \tag{10}$$

Where:

C_T: Total capacitance of the structure; L_T: Total inductance of the structure.

Total capacitance (C_T) and inductance (L_T) are found by connecting the series and shunt branches of the capacitances (C1 to C6) and inductances (L1 to L5) in series and/or parallel.

In MRSRR, metal strips are assumed to be inductors, while splits act as capacitors. When MTM cells are excited using electromagnetic waves, two kinds of coupling are observed: Coupling between the splits (gaps) and the electric field generates electric resonances, and the magnetic field couples with rings (strips), which produces magnetic resonances.

Researchers operate an equivalent circuit representing a structure's qualitative response to understand or estimate how an electrical circuit will resonate across various resonant frequencies [26]. Figure 8 shows the optimized equivalent circuit for the MRSRR unit cell. It consists of the passive elements L and C that introduce the triple resonance frequencies.

G1 and G2 are the critical parameters determining resonance mode in the proposed MRSRR. In equivalent circuit analysis, a gap G1 could be modeled by two series-connected capacitors, C1 and C2, with an inductor L1 at its middle, thus forming an LC resonant circuit. Variations of G1 adjust the capacitance value and, therefore, may change resonance frequency and field distribution. C3 and

C4 correspond to G2 in the upper and lower halves. Besides, they alter the coupling between resonators; hence, their variation affects resonance characteristics.

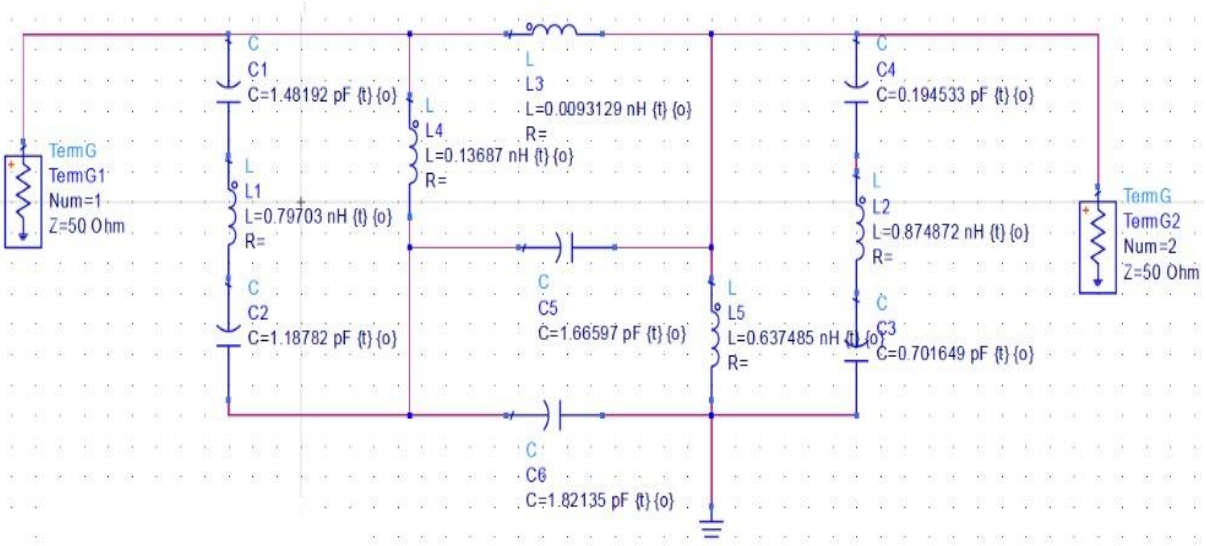

Figure 8. The equivalent circuit model of the MRSRR-MTM cell.

Similarly, G2 can be pictured as C3 and C4 at upper and lower, respectively. More precisely, they toggle between resonators, couplings, and resonance characteristics. Changing the gap parameters will change the distribution of the electromagnetic field. Hence, the coupling strength in adjacent resonators will change; thus, the resonance properties, including the excitation mode, will vary.

Chao and Chau [27] clarified that properly tuned geometric parameters, such as the gap sizes in split-ring resonators, can improve both the field confinement and nonlinear interactions. Further, they found that the effective nonlinear susceptibilities in metasurfaces for split-ring resonators in resonance tuning can be enhanced by carefully adjusting the gap size, significantly strengthening the SHG process.

To achieve results closer to the ones using CST simulations, the values of the analogous circuit components varied within Agilent's ADS software. Magnitude S_{21} derived from two electromagnetic tools, CST and ADS, is compared in Figure 9. The corresponding circuit delivered three resonance frequencies with maxima of -49.94 dB, -44.12 dB, and -43.98 dB at 5.63 GHz, 8.55 GHz, and 13.88 GHz, respectively. It is important to note that three stopbands below -30 dB were presented from the ADS simulation. The identified regions demonstrated significant concordance, reinforcing the analogous circuit's validity.

Table 3 compares the transmission coefficient and resonance frequency obtained from CST and ADS, clearly presenting the results. We also calculated the frequency shift for each of the three frequencies, which yielded a difference of less than 2%, supporting the accuracy of the ADS result.

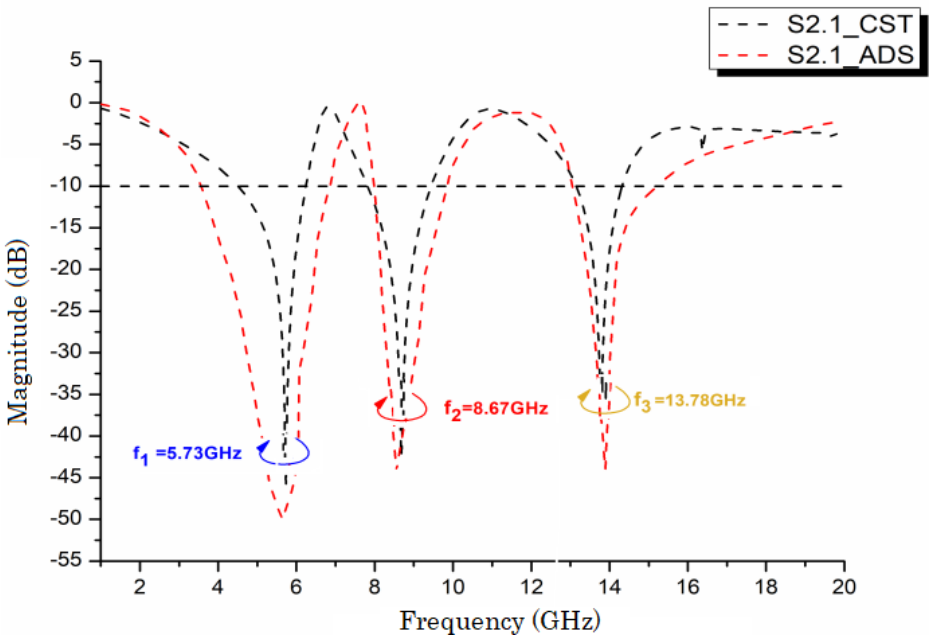

Figure 9. Transmission coefficient S_{21}, as by CST and ADS.

Table 3. S_{21} Comparison between CST and ADS for MRSRR-MTM cell.

	Peaks [dB] at res. Freq. [GHz]	Shifts [%]
CST	-46.01 dB at 5.73 GHz -42.49 dB at 8.67 GHz -35.93 dB at 13.78 GHz	1.76 1.39 0.72
ADS	-49.94 dB at 5.63 GHz -44.12 dB at 8.55 GHz -43.98 dB at 13.88 GHz	

3.4. Array analysis

Unit cells alone cannot exhibit the correct exotic electromagnetic properties of metamaterials. Usually, for a multiunit cell MTM to have desirable exotic electromagnetic properties, several unit cells rather than a single unit cell must be used. MTM with electrically conducted components is usually an array possessing adequate capacitive and inductive characteristics.

Various types of array designs were simulated and analyzed; some array types that attracted interest include 1 ×2, 2 ×1, 2 ×2, and 4 ×4 arrays, as shown in Figure 10(a-d). Selected arrays were numerically simulated in the frequency range [1-20 GHz] using CST 3D-EM, following the same method as the primary unit cell. Note that the unit cells are positioned both horizontally and vertically with a distance of 0.5 mm between each other.

Figure 11 shows the transmission coefficient results for the selected array types. From Figure 11(a), we can observe that resonance frequencies of the basic unit cell are roughly the same as the S_{21} results of the 1 ×2 array, with just 2.11%, 0.69%, and 0.58% shifts, respectively.

Figures 11(b-c) show that S_{21} results for 2 ×1 and 2 ×2 arrays presented five resonant frequencies around 4, 6, 7, 9, and 13 GHz with magnitude below -20 dB. Compared to the basic unit cells, two resonant frequencies appeared due to the capacitive effect on the nearby unit cells. New resonances have emerged from new stop bands in the 1 to 20 GHz frequency band. For the 4 ×4

array, S_{21} curves indicate five peaks below -20 dB. Note that the two first resonances have emerged to give one at 6.24 GHz with a broader bandwidth from 4.3 to 6.56 GHz, as illustrated in Figure 11(d). S_{21} results exhibited the same resonance at 7.19, 9.23, and 13.39 GHz regarding the third, fourth, and fifth frequencies, respectively. Moreover, 13.78 GHz for the basic unit cell was the only frequency maintained around 13 GHz, with a slightly lower shift. The mutual coupling effect was responsible for the appearance of a new resonance frequency and the change between resonances.

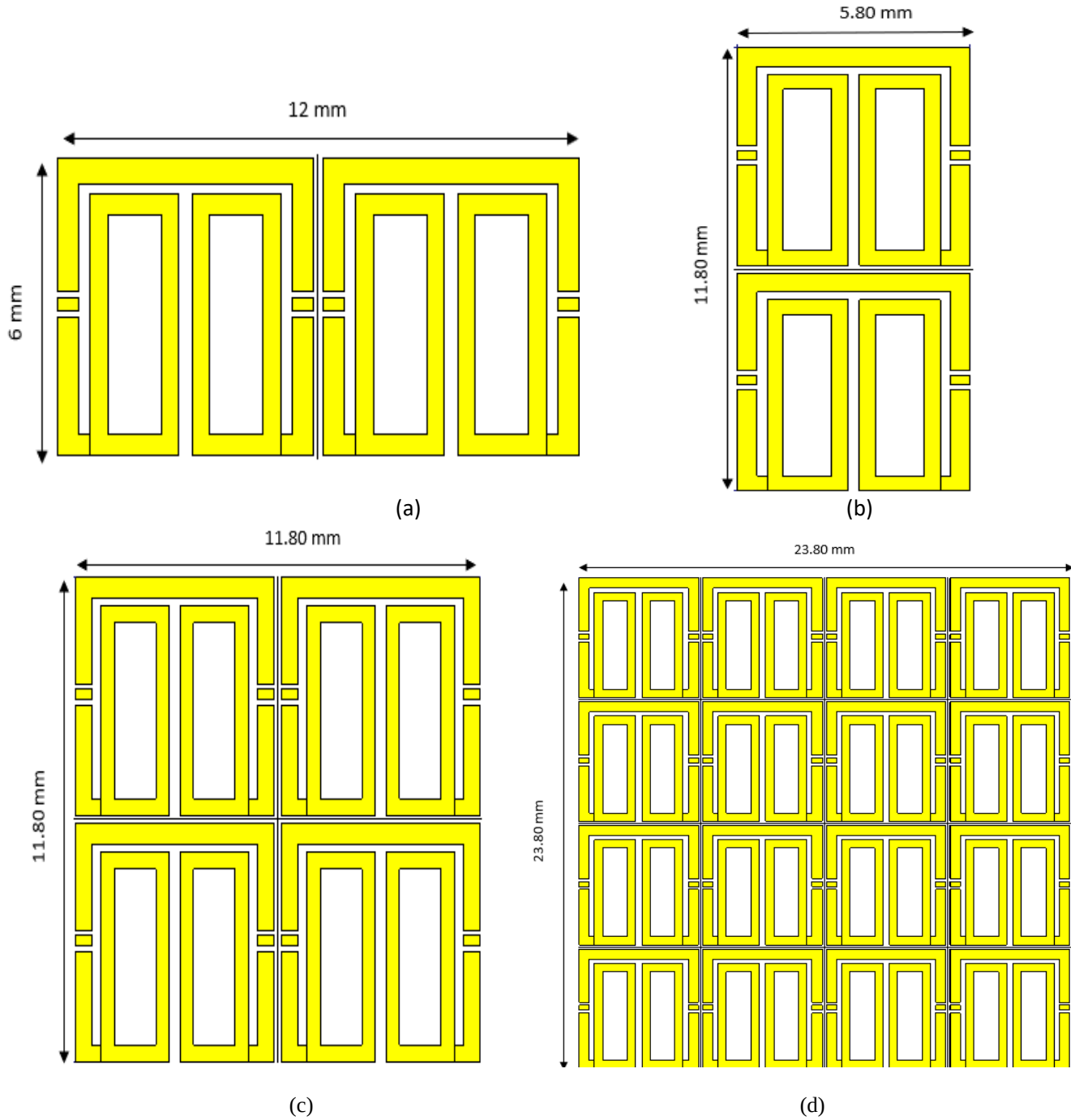

Figure 10. Different array configurations based on MRSRR unit cell (a) 1 × 2, (b) 2 × 1, (c) 2 × 2, and (d) 4 × 4.

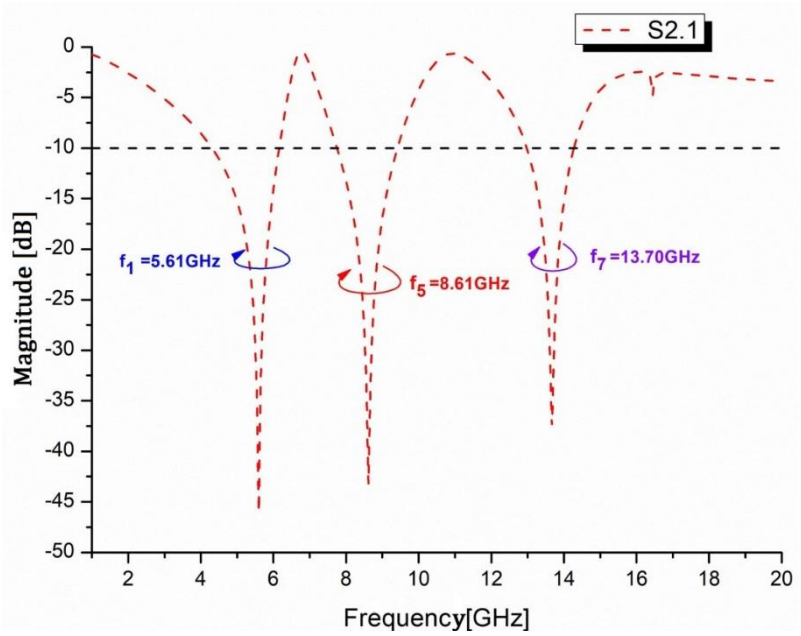

(a)

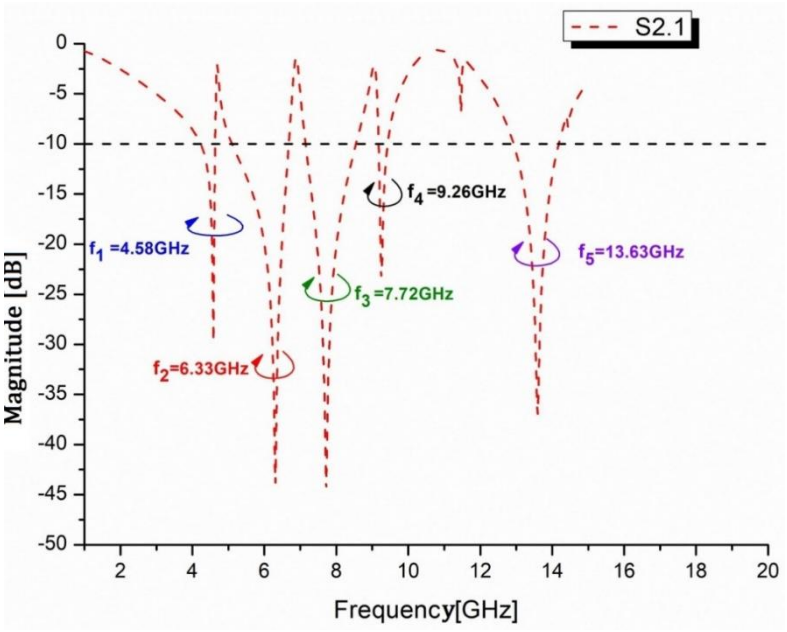

(b)

Figure 11. Transmission coefficients plot using different types of arrays (a) 1 × 2, (b) 2 × 1, (c) 2 × 2, and (d) 4 × 4.

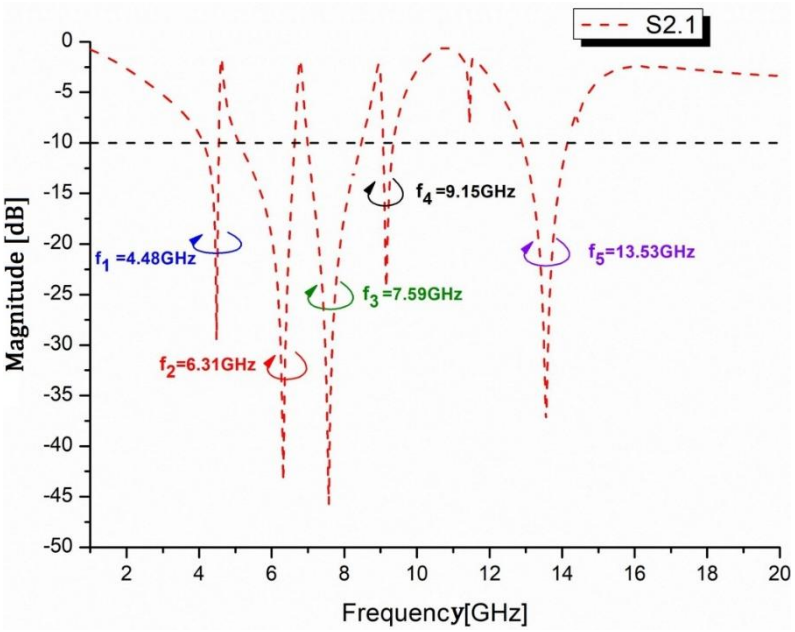

(c)

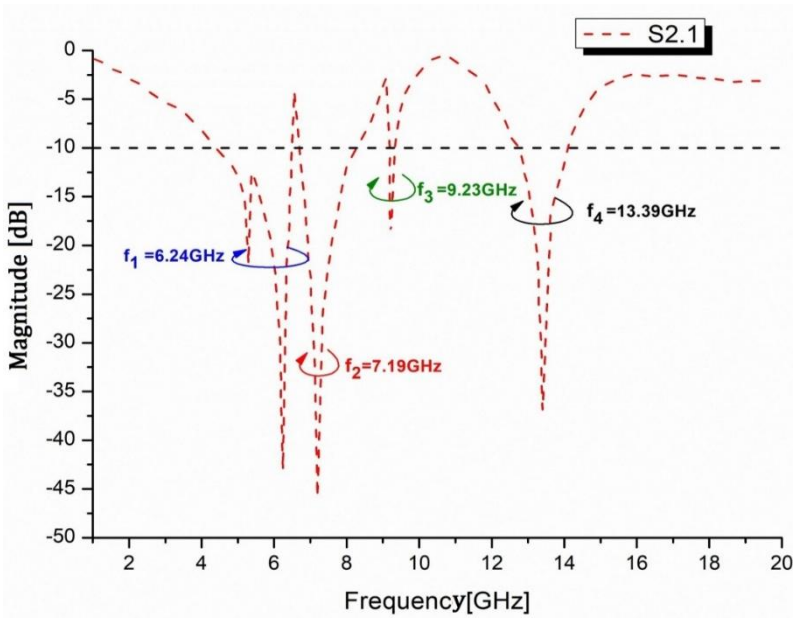

(d)

Figure 11. Continued.

Figures 12(a-b) and (c-d) show the real permittivity and permeability values as a function of the frequency of the selected array structures. We observed that the plotted curves of the effective parameters for the 1 × 2 and 2 × 1 array structures were nearly identical. However, there was a discrepancy between the negative values. The same observation was valid for the 2 × 2 and 4 × 4 array structures.

The modification in S-parameters (S_{11}, S_{21}) was the primary reason for the observed disparity in the negative values, as shown in Figure 11. Equations (8) and (9) are practically based on the computation of electromagnetic properties (permittivity and permeability), with S_{11} and S_{21} serving as crucial parameters (for more information, see equations (6) and (7)). The negative value shift

illustrated in Figures 12(a-b) and 12(c-d) results from any alteration in these S-parameters, which can directly affect the electromagnetic characteristics produced as an influence.

Table 4 presents an analysis of the features of various array structures, including the type of MTM (ENG, MNG, DNG), the frequency band, and the satellite band under consideration. 2 ×2 and 4 ×4 array structures have shown three features (ENG, MNG, and DNG) in the [1-20 GHz] frequency band. MNG feature has been disregarded by 1 ×2 and 2 ×1. It is observed that the structure of the 4 ×4 array antenna covers both the C and X bands, while the 1 ×2, 2 ×1, and 2 ×2 array antenna structures cover the Ku band.

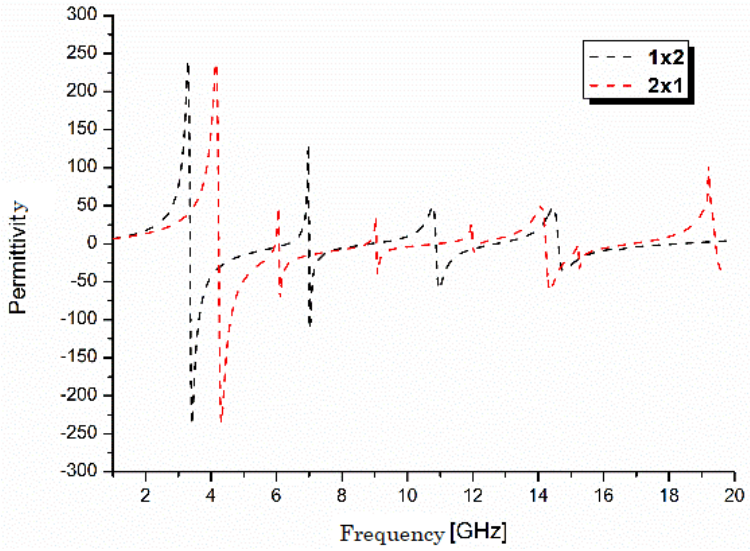

(a)

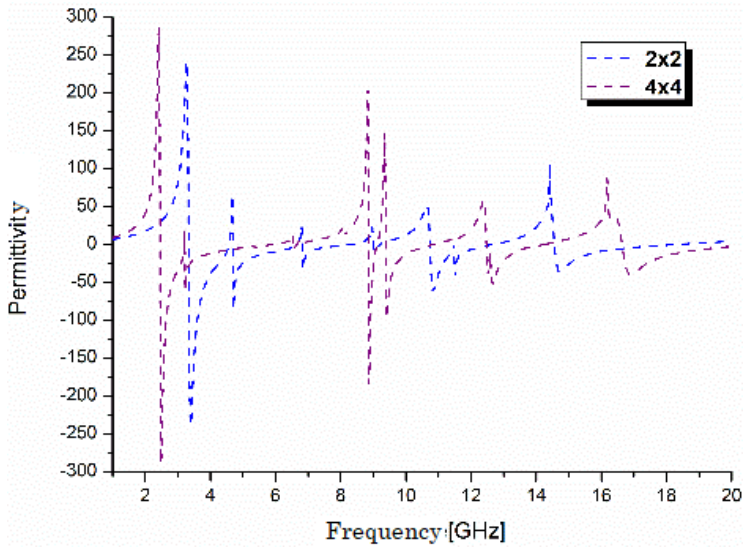

(b)

Figure 12. (a, b) Real values of effective permittivity (ε) versus frequency, and (c, d) effective permeability (μ) versus frequency.

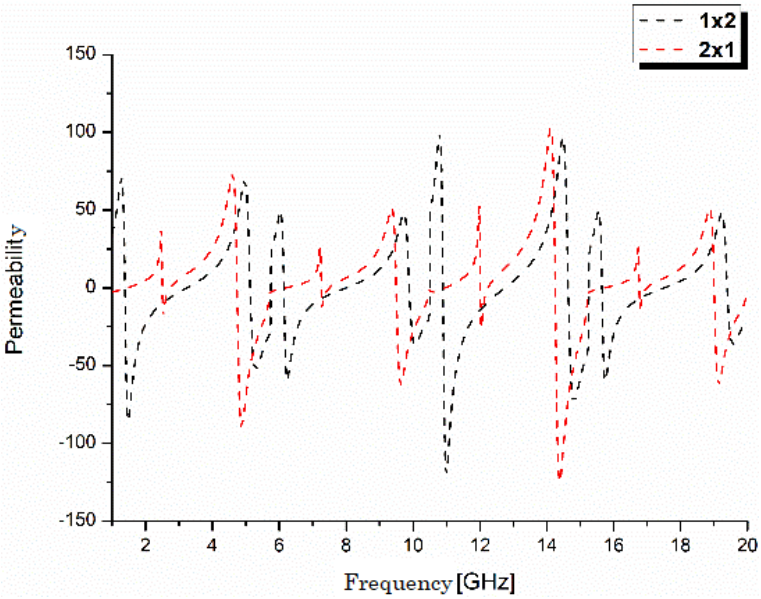

(c)

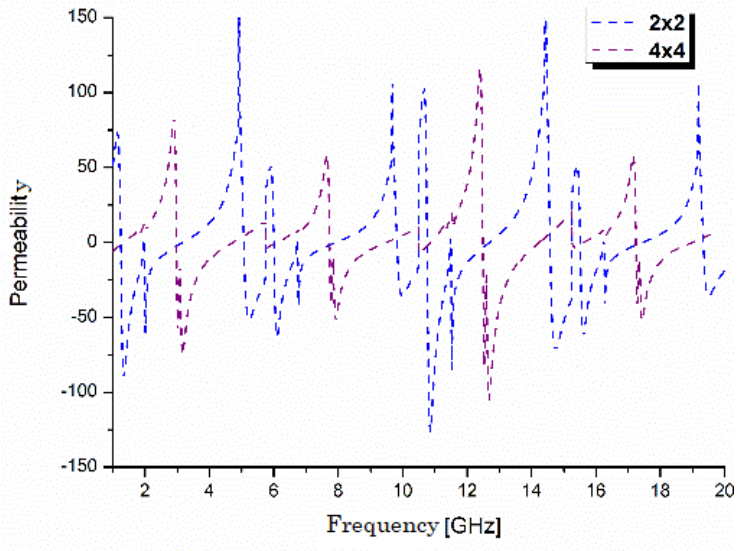

(d)

Figure 12. Continued.

Table 4. Array structure characteristics.

Array structures	Type of metamaterial	Frequency band [GHz]	Satellite band covered
1×2	ENG	[5.76 – 6.14], [8.01 – 8.80]	C and X
	MNG	/	
	DNG	[4.33 – 5.75], [7.76 – 8.00],	
2×1	ENG	[4.17 – 4.63], [6.07 – 6.69], [7.16 – 7.25], [7.47 – 8.55], [9.18 – 9.42]	C and X
	MNG	[5.99 – 6.10]	
	DNG	[5.10 – 5.98], [7.26 – 7.46]	
2×2	ENG	[4.17 – 4.55], [5.76 – 6.00], [7.96 – 8.20], [9.07 – 9.19]	C and X
	MNG	/	
	DNG	[5.10 – 5.75], [6.01 – 6.63], [6.99 – 7.95]	
4×4	ENG	[4.73 – 5.75]	C, X and Ku
	MNG	[5.85 – 6.09], [7.72 – 8.25], [9.18 – 9.32], [12.49 – 12.64]	
	DNG	[4.41 – 4.72], [5.76 – 5.84], [12.65 – 14.11]	

4. Comparative analysis

Table 5 contrasts several recent studies with the suggested unit cell on dimension, band covered, type of metamaterial, effective medium ratio (EMR), and the extraction method. The comparison shows that the proposed MRSRR has a more compact size than the previous studies, except [1]. However, the cell presented in [1] covered only the Ku band, with unique character (DNG) and a lower EMR. Comparatively, the proposed cell covered C, X, and Ku bands, demonstrating ENG, MNG, and DNG characters. Further, EMR that represents the compactness of unit cells is higher than [1], [10], and [26]. Thus, all studies use the NRW method to extract effective parameters except [28], which used the Smith method.

Table 5. MRSRR unit cell vs previous studies.

Ref./ Year	Dimension (mm^2)	Satellite band covered	Type of MTM	EMR	Extraction method
[1/2022]	3.05 × 2.85	Ku	DNG	3.76	NRW
[9/2023]	10 × 10	C, X, Ku	ENG	4.5	NRW
[12/ 2016]	12 × 12	C, X, Ku	DNG	15.33	NRW
[13/2020]	9 × 9	S, X, Ku	DNG	11.51	NRW
[26/2016]	8 × 8	C, Ku	MNG	6.47	NRW
[29/2020]	8 × 8	S, C, X	DNG	13.11	NRW
[30/2021]	10 × 10	S, C, X	ENG	12.61	Smith
[31/2022]	10 × 10	S, C, Ku	ENG	14.85	NRW
[32/2022]	11 × 11	S, C, X, Ku	MNG	13.5	NRW
This work	6 × 6	C, X, Ku	ENG, MNG, DNG	8.72	NRW

5. Conclusions

We focus on developing and investigating rectangular split-ring resonator (SRR) unit cells designed to exhibit epsilon-negative (ENG), double-negative (DNG), and mu-negative (MNG) characteristics across the satellite frequency ranges. The proposed unit, designed on Rogers RO3006 substrate with a compact footprint of 6 × 6 mm^2, was modeled using CST software, yielding resonance frequencies at 5.73 GHz, 8.67 GHz, and 13.78 GHz. The metamaterial properties were extracted using the Nicolson-Ross-Weir (NRW) method, demonstrating negative permeability in the Ku-, double-negative behavior in the X-, and negative permittivity in the C-band. Stopband characteristics were further analyzed by visualizing the surface current distribution at the resonance frequencies.

The ADS simulator generates the corresponding circuit model, and S_{21}'s response nearly corresponds to the CST output. Following, the comparison of 1 × 2 and 2 × 1 and 2 × 2 and 4 × 4 arrays conducted where appropriate commitment to the effective parameters is confirmed. Therefore, the proposed MRSRR unit cell applies to satellite applications over the C-, X-, and Ku ranges. C-band frequency range is used for full-time satellite TV networks, radar applications, and weather monitoring. X-band satellite communication finds use in the military for defense tracking, air traffic control, and radar applications. Also, the Ku-band is used as a direct broadcast satellite service.

While allowing a size decrease, the suggested MRSRR can improve the performance parameters of microwave circuits, including gain and directivity. By reconfiguring, the suggested metamaterial unit cell can be improved overall performance-wise, and its coverage of satellite band frequencies can be expanded.

The research presented in this study primarily relies on simulations. However, considering any manufacturing problems for the suggested metamaterials is essential. One of the major difficulties is manufacturing with the needed accuracy to assure homogeneity in unit cell forms. At high frequencies such as millimeter waves, where exact tolerances are crucial, even small size changes can significantly influence electromagnetic (EM) properties. This topic has become highly available for modern methods of communication, including 5G millimeter-wave networks. Alam and Latif also consider some problems manufacturing the 5G double-split rectangular dual-ring metamaterial [1].

Another fabrication issue is that, when adding conductive elements to the design, the structural integrity of the metamaterial is sacrificed. Indeed, conductive elements must be fabricated and shrunk precisely, or they will not retain integrity and functionality. This issue is most relevant with metamaterials designed to operate at microwave and millimeter-wave frequencies, as Islam et al. noted in their efforts to develop three-band microwave CCSRR metamaterial [30].

One of the prime considerations in any building process involves the choice of substrate material because the dielectric characteristics of the substrate are bound to affect the general performance of the metamaterial. Accordingly, Hossain et al. demonstrate a modified split-ring resonator design with a high effective medium ratio for satellite communication applications [12]. In contrast, Hussain et al. describe issues concerning several bands in using DNG metamaterials [21]. The authors emphasize the urgent need for precise tuning of the characteristics of the materials for the attainment of desired electromagnetic responses.

Author contributions

Abderraouf Fadhel, Souad Berhab and Abdennour Belhedri: Investigation, Writing – original draft, Writing – review & editing; Hassene Mnif and Rahma Aloulou: Writing – review & editing, Resources. All authors have read and agreed to the published version of the manuscript.

Conflict of interest

The author declares that there is no conflict of interest in this paper.

References

1. Alam MJ, Latif SI (2022) Double-Split Rectangular Dual-Ring DNG Metamaterial for 5G Millimeter Wave Applications. *Electronics* 12: 174. https://doi.org/10.3390/electronics12010174
2. Buriak IA, Zhurba VO, Vorobjov GS, Kulizhko VR, Kononov OK, Rybalko O (2016) Metamaterials: Theory, Classification and Application Strategies. *J Nano- Electron Phys (Ukraine)* 8: 04088-1-04088-11. https://doi.org/10.21272/jnep.8(4(2)).04088
3. Alibakhshikenari M, Virdee BS, Elwi TA, Lubangakene ID, Jayanthi RK, Al-Behadili AA, et al. (2023) Design of a Planar Sensor Based on Split-Ring Resonators for Non-Invasive Permittivity Measurement. *Sensors* 23: 5306. https://doi.org/10.3390/s23115306
4. Abderrahim Annou (2022) *Contribution to the design and optimization of compact reconfigurable antennas based on metamaterials: wireless and body communications*, PhD dissertation, electron and telecom, univ of Ouargla, Algeria.
5. Nasiri B, Errkik A, Zbitou J (2021) A new design of stepped antenna loaded metamaterial for RFID applications. *Bulletin of Electrical Engineering and Informatics* 10: 2661–2666. https://doi.org/10.11591/eei.v10i5.2675
6. Urul B (2020) Gain enhancement of microstrip antenna with a novel DNG material. *Microw Opt*

Techn Lett 62: 1824–1829. https://doi.org/10.1002/mop.32240
7. Hossain MJ, Faruque MR, Islam MT (2018) Perfect metamaterial absorber with high fractional bandwidth for solar energy harvesting. *PLoS One* 13: e0207314. https://doi.org/10.1371/journal.pone.0207314
8. Ma S, Zhang P, Mi X, Zhao H (2023) Highly sensitive terahertz sensor based on graphene metamaterial absorber. *Opt Commun* 528: 129021. https://doi.org/10.1016/j.optcom.2022.129021
9. Mohammed B, Özkaya U, Kobibi YID, Zouggaret A, Hebali M (2023) A Novel Dual-band Bandpass Metamaterial Filter using Ground Plane Demetallization Technology for Wireless Communications Applications. *ICFAR 2023* 1: 530–534. Available from: https://as-proceeding.com/index.php/icfar/article/view/158
10. Hasan MM, Faruque MR, Islam SS, Islam MT (2016) A New Compact Double-Negative Miniaturized Metamaterial for Wideband Operation. *Materials* 9: 830. https://doi.org/10.3390/ma9100830
11. Islam MS, Islam MT, Sahar NM, Rmili H, Amin N, Chowdhury ME (2020) A mutual coupled concentric crossed-Line split ring resonator (CCSRR) based epsilon negative (ENG) metamaterial for Tri-band microwave applications. *Results Phys* 18: 103292. https://doi.org/10.1016/j.rinp.2020.103292
12. Hossain MB, Faruque MR, Islam SS, Islam MT (2021) Modified double dumbbell-shaped split-ring resonator-based negative permittivity metamaterial for satellite communications with high effective medium ratio. *Sci Rep* 11: 19331. https://doi.org/10.1038/s41598-021-98703-4
13. Al-gburi AJ, Ibrahim IM, Abdulhameed MK, Zakaria Z, Zeain MY, Keriee HH, et al. (2021) A compact UWB FSS single layer with stopband properties for shielding applications. *Przegląd Elektrotechniczny* 2: 165–168. https://doi.org/10.15199/48.2021.02.34
14. Sharma A, Singh H, Gupta A, Al-Gburi AJ (2024) Development and evaluation of wideband negative response in ultra-thin polygon metamaterial. *Eur Phys J B* 97: 61. https://doi.org/10.1140/epjb/s10051-024-00692-6
15. Sabaruddin NR, Tan YM, Chou Chao CT, Kooh MR, Chou Chau YF (2024) High Sensitivity of Metasurface-Based Five-Band Terahertz Absorber. *Plasmonics* 19: 481–493. https://doi.org/10.1007/s11468-023-01989-5
16. Chou Chau YF (2024) Boosting Second Harmonic Generation Efficiency and Nonlinear Susceptibility via Metasurfaces Featuring Split-Ring Resonators and Bowtie Nanoantennas. *Nanomaterials* 14: 664. https://doi.org/10.3390/nano14080664
17. Alam MJ, Faruque MR, Azim R, Islam MT (2018) Depiction and analysis of a modified H-shaped double-negative meta-atom for satellite communication. *Int J Microw Wireless Technol* 10: 1155–1165. https://doi.org/10.1017/S1759078718001022
18. Hossain MI, Faruque MR, Islam MT, Ullah MH (2014) A New Wide-Band Double-Negative Metamaterial for C- and S-Band Applications. *Materials* 8: 57–71. https://doi.org/10.3390/ma8010057
19. Islam MS, Samsuzzaman M, Beng GK, Misran N, Amin N, Islam MT (2020) A Gap Coupled Hexagonal Split Ring Resonator Based Metamaterial for S-Band and X-Band Microwave Applications. *IEEE Access* 8: 68239–68253. https://doi.org/10.1109/ACCESS.2020.2985845
20. Almutairi AF, Islam MS, Samsuzzaman M, Islam MT, Misran N, Islam MT (2019) A complementary split ring resonator-based metamaterial with effective medium ratio for C-band microwave applications. *Results Phys* 15: 102675. https://doi.org/10.1016/j.rinp.2019.102675
21. Hussain A, Dong J, Abdulkarim YI, Wu R, Muhammadsharif FF, Shi R, et al. (2023) A double negative (DNG) metamaterial based on parallel double-E square split resonators for multi-band

applications: Simulation and experiment. *Results Phys* 46: 106302. https://doi.org/10.1016/j.rinp.2023.106302

22. Al-Taie RR, Ali MM, Tawfeeq OA, Al-Adhami Y, Ghazi HS, Noori NM, et al. (2022) On the Performance of a Composite Right Left Hand Electromagnetic Bandgap Structure. *2022 9th International Conference on Electrical Engineering, Computer Science and Informatics (EECSI)*, 420–423. https://doi.org/10.23919/EECSI56542.2022.9946487
23. Ashyap AY, Dahlan SH, Abidin ZZ, Abbasi MI, Kamarudin MR, Majid HA, et al. (2020) An Overview of Electromagnetic Band-Gap Integrated Wearable Antennas. *IEEE Access* 8: 7641–7658. https://doi.org/10.1109/ACCESS.2020.2963997
24. Berhab S, Annou A, Ammari A, Bouidia I (2021) Reconfigurable single to multi-band bandstop pcsrrs-based filter: Analysis and circuits modeling. *Telecommunication and Radio Engineering* 80. https://doi.org/10.1615/TelecomRadEng.2022040621
25. Smith DR, Vier DC, Koschny T, Soukoulis CM (2005) Electromagnetic parameter retrieval from inhomogeneous metamaterials. *Phys Rev E* 71: 036617. https://doi.org/10.1103/PhysRevE.71.036617
26. Hasan MM, Faruque MR, Islam SS, Islam MT (2016) A New Compact Double-Negative Miniaturized Metamaterial for Wideband Operation. *Materials* 9: 830. https://doi.org/10.3390/ma9100830
27. Chao CT, Chau YF (2024) Enhancing second harmonic generation efficiency and effective nonlinear susceptibility via metasurfaces employing split-ring resonators. *Opt Commun* 562: 130568. https://doi.org/10.1016/j.optcom.2024.130568
28. Annou A, Berhab S, Chebbara F (2020) Metamaterial-Fractal-Defected Ground Structure Concepts Combining for Highly Miniaturized Triple-Band Antenna Design. *Journal of Microwaves, Optoelectronics and Electromagnetic Applications* 19: 522–541. https://doi.org/10.1590/2179-10742020v19i4894
29. Ramachandran T, Faruque MR, Islam MT (2020) A dual band left-handed metamaterial-enabled design for satellite applications. *Results Phys* 16: 102942. https://doi.org/10.1016/j.rinp.2020.102942
30. Islam MR, Islam MT, Soliman MS, Baharuddin MH, Mat K, Moubark AM, et al. (2021) Metamaterial based on an inverse double V loaded complementary square split ring resonator for radar and Wi-Fi applications. *Sci Rep* 11: 21782. https://doi.org/10.1038/s41598-021-01275-6
31. Afsar MS, Faruque MR, Khandaker MU, Alqahtani A, Bradley DA (2022) A New Compact Split Ring Resonator Based Double Inverse Epsilon Shaped Metamaterial for Triple Band Satellite and Radar Communication. *Crystals* 12: 520. https://doi.org/10.3390/cryst12040520
32. Hossain MB, Faruque MR, Islam MT, Khandaker MU, Tamam N, Sulieman A (2022) Modified Coptic Cross Shaped Split-Ring Resonator Based Negative Permittivity Metamaterial for Quad Band Satellite Applications with High Effective Medium Ratio. *Materials* 15: 3389. https://doi.org/10.3390/ma15093389

AIMS Press